Enabling Thermal Energy Storage in Structural Cementitious Composites with a Novel Phase Change Material Microcapsule Featuring an Inorganic Shell and a Bio-inspired Silica Coating

Abdulmalik Ismail [1], Maysam Bahmani [1], Xiaodong Wang [1], Anastasia Aday [2], Adewale Odukomaiya [2], Jialai Wang [1*]

[1] Department of Civil, Construction and Environmental Engineering, The University of Alabama, Tuscaloosa, AL 35487, USA.

[2] National Renewable Energy Laboratory, USA.

Abstract

Phase change material (PCM) microcapsules offer a promising approach for integrating PCM into building materials for efficient thermal energy storage. This study presents the development of a novel PCM microcapsule specifically designed for incorporation into cementitious materials. The microcapsule consists of a low-cost PCM core derived from vegetable oil by-products and a durable inorganic shell made from cenosphere, a hollow fly ash generated from coal burning power plants. A novel process is developed to apply a silica coating to these cenosphere-based PCM microcapsules (CPCM), resulting in bioinspired-silica-coated CPCM microcapsules (BCPCM). This coating process draws inspiration from marine microorganism-based silica production and utilizes low-cost sodium silicate as a precursor, enabling eco-friendly and cost-effective manufacturing at ambient temperature and mild pH conditions. The morphology, chemical stability, and thermal properties of the BCPCM along with its thermo-mechanical performance in cementitious composites were comprehensively analyzed. Experimental results demonstrate successful silica deposition on BCPCM, leading to enhanced latent heat properties of the produced BCPCM. With the silica coating, BCPCM exhibits a 50°C delay in thermal decomposition compared to CPCM, enhancing fire resistance and preventing premature PCM leakage of the microcapsule. The bioinspired silica coating effectively restores over 10% of the strength loss for each percent increase in CPCM incorporated into the mortar. The thermal performance experiments reveal that increasing the BCPCM content reduces temperature peaks and rates of temperature increase, indicating an improved capacity for thermal energy

*Corresponding author.

Email address: jwang@eng.ua.edu (J. Wang).

storage. This new PCM microcapsule provides a cost-effective solution to integrate thermal energy storage to cementitious material, as evidenced by that over 30% aggregates (in volume) can be replaced by the microcapsule without drastically loss of strength.

1. Introduction

Phase change materials (PCM) are essential for thermal energy storage (TES) in buildings due to their unique ability to store and release large amounts of energy during phase transitions. However, directly incorporating PCM into building materials often faces challenges, including potential chemical interactions, uneven dispersion, leakage, and compromised durability. Microencapsulation addresses these challenges by providing a protective shell around the PCM, preventing direct contact with the building material matrix. Microencapsulation ensures that PCM remains securely contained, prevents leakage or degradation, and enables controlled release of thermal energy when required, making it a preferred approach for incorporating PCMs into building materials for thermal energy storage. Additionally, it allows for easy incorporation into various products, such as textiles, building materials, and thermal energy storage systems.

In the existing literature, majority of PCM microcapsules use polymer shell due to its versatility in encapsulating various PCMs, and highly efficient containment [1]. For instance, Borreguero et al.[2] employed the spray drying method to encapsulate paraffin wax RT27 within a polyethylene-ethylvinylacetate polymer shell. Li et al. [3] produced copolymer microcapsules with various concentrations of n-octadecane PCM by suspension-like polymerization. Enteshari et al. [4] developed melanin formaldehyde microcapsules via emulsion polymerization. Liu et al. [5] used in-situ polymerization to create microcapsules with phenol-formaldehyde resin shell. These polymeric shells often suffer from some limitations, such as low thermal conductivity [6], inadequate mechanical strength/stiffness [7], potential degradation at high temperature, and potential environmental concerns. The insufficient strength of existing microencapsulated PCMs (MPCMs) makes them prone to damage or breakage when subjected to impacts during handling [8]. These limitations of polymeric MPCMs rendered them unsuitable for applications that require high strength, such as concretes.

To address these constraints, substantial studies have been devoted to investigating inorganic microcapsules with higher mechanical strength/stiffness and thermal conductivity. Various inorganic materials such as ZnO [9] , TiO_2 [10], SiO_2 [11], and $CaCO_3$ [12], have been used to microencapsulate PCMs and resulting MPCMs exhibit better thermomechanical performance than the ones with organic polymeric shells. Among these inorganic materials, SiO_2 shells are widely employed, particularly when incorporating MPCMs into cementitious composites. This is because potential reaction between the silica microcapsule and calcium hydroxide produced by cement hydration can produce more calcium silicate hydrate (C-S-H) gel, which can increase the bond strength between the microcapsule and cement paste [13], [14]. More importantly, silica-based microcapsules have much higher thermal conductivity than the polymer-based ones [15], thereby enhancing their capacity to store and release energy during phase transitions. However, inorganic shells also have some limitations. The synthesis of inorganic-shell microcapsules often involves more complex and sophisticated processes compared to organic polymers, making it more expensive than the organic shell. Inorganic shell may not be compatible with all types of PCMs, and therefore, is susceptible to separation from PCM, and cannot withstand the volume change stress resulting from repeated thermal cycles [16]. Therefore, additional research is required to tackle these obstacles and create durable microcapsules capable of meeting the requirements of real-world applications.

Our previous research adopted cenosphere, hollow microspheres with excellent mechanical strength and thermal conductivity, to encapsulate PCM to produce a cenosphere-based PCM microcapsule (CPCM) [15]. Since the complicated synthesis process from expensive pre-cursors for the inorganic shell is eliminated, CPCM offer a much higher cost-effective solution to for microencapsulation with inorganic shell. To prevent leaking of liquid PCM from the cenosphere shell and enhance the bonding between the cenosphere and cement matrix, a silica coating can be applied on the surface of the CPCM. Although the resulting silica coating on the surface CPCM exhibits excellent compatibility with the cement matrix [15], it drastically reduces the encapsulation efficiency of the microcapsule due to the heavy, and uneven silica layer significantly increasing the mass of the microcapsule. This silica coating can be improved by the sol-gel method. However, sol-gel method requires more expensive precursors, harsh processing conditions, and many highly toxic chemicals.

Aiming to overcome the limitations of existing methods to apply silica coating, this study took inspiration from the natural synthesis process of silica. Organisms such as sponges and diatoms are known to produce intricately structured silica formations on a considerable scale. This process takes place under mild pH and at ambient temperatures and is regulated by proteins [17]. Taking cues from this bio-silicification process, we explored the use of biomolecules including proteins and peptides to induce the in vitro production of silica. By adding silaffin proteins to a silica precursor solution, Sumper et al. [18] demonstrated the rapid precipitation of silica under almost neutral pH and ambient temperature conditions. Silaffins are peptides that undergo post-translational modifications, with lysine residues modified to allow for coupling with long-chain polyamines [19]. The assembled polyamine structure of silaffins serves as a catalytic template for polycondensation of silicic acid derivatives in diatoms. As a result, silica films can be easily applied to various substrates by first introducing a layer of polyamine as a mimic of silaffins on the surface and then submerged in silica precursor solution [20]. By mimicking this silica film formation process, this study developed a novel, scalable, and cost-effective approach to apply silica coating on the surface of CPCM. This coating process is carried out under mild pH value and ambient temperature conditions, minimizing production costs and toxic waste. More importantly, better quality of the coating can be achieved.

The microstructural morphology, chemical compatibility, and thermal properties of the CPCM and BCPCM were characterized using advanced techniques such as scanning electron microscopy (SEM), energy dispersive spectroscopy (EDS), Fourier transform infrared spectroscopy (FTIR), thermogravimetric analysis (TGA), derivative thermogravimetry (DTG), and differential scanning calorimetry (DSC). Mortar samples were prepared by incorporating varying volume percentages of CPCM and BCPCM and then subjected to comprehensive evaluations of their mechanical and thermal properties. Finally, the potential of BCPCM on TES application was evaluated with cementitious composites incorporating different volume fractions of BCPCM.

2. Materials and methods

Cenosphere ES 160 purchased from Cenostar Corporation, USA, and type I Portland cement purchased from Sakrete (USA) were used in this study. A biobased PCM, PureTemp 29, produced by PureTemp, USA was used as the core material. The thermophysical properties of PureTemp 29 are shown in Table 1. Ammonium fluoride (NH_4F) with a purity of 96% was purchased from Beantown Chemical Corporation (USA). Hydrochloric acid (HCl), sodium metasilicate nonahydrate were commercially obtained from MP biomedicals, USA. Sodium phosphate dibasic heptahydrate and sodium phosphate monobasic monohydrate were ordered from VWR International, USA. Poly (allylamine hydrochloride) (PAH) and Lysozyme were purchased from Thermo Fisher, USA. Calcium gluconate gel was readily available for safety purposes during acid etching.

Table 1: Properties of biobased PCM from manufacturer

Melting temperature (°C)	Latent heat (J/g)	Thermal conductivity (W/m°C)	Density (solid/liquid) (g/ml)	Specific heat (J/g °C)
29	202	0.25/0.15	0.94/0.85	1.77/1.94

2.1 Production of CPCM

The manufacturing process of CPCM, schematically shown in Fig. 1, has been thoroughly discussed in our previous study [15]. The as received cenospheres were soaked in water for 30 min under vacuum for 1h. The broken cenospheres sank and the unbroken cenospheres floating at the top were collected for chemical etching. 25g of the collected cenospheres were soaked in 250 ml of 1.0M NH_4F-1.2M HCl-H_2O solution for 1.5h with occasional stirring at 15 min intervals. At the beginning, the cenospheres floated on the etching solution. The hydrofluoric acid (HF) produced in the chemical etching process dissolved the glassy films covering the cenospheres to create perforations through which melted PCM can be loaded. The etched cenosphere sank at the bottom due to the increased density from the inflow of etching solution into the cenosphere. The etched cenospheres were vacuum filtered, washed many times with water until the pH of the solution was neutral and then oven dried at 105ºC for 48h. The PCM was loaded into the etched cenospheres by the vacuum encapsulation method. To do this, 50g of etched cenospheres were firstly placed under vacuum pressure of approximately 88 kPa for 30 mins to remove trapped air in the chamber and cenospheres. Then about 300ml of melted PCM, corresponding to approximately 3 times the volume of the etched cenosphere was quickly introduced into the vacuum chamber under the same pressure and 70oC for 2h. Vacuum was then removed, and air was allowed back in to push the PCM through the perforations on the cenospheres under gravity. The produced microcapsule, CPCM, was vacuum filtered and then cooled below room temperature to ensure the encapsulated PCM to solidify. The excess PCM filtered from the loading process was reused for another CPCM production process thereby zeroing out any PCM waste. The produced CPCM microcapsules were then rinsed with 40oC water to remove residual PCMs on the surface, followed instantly by cooling in iced water to prevent leakage of encapsulated PCM. The resulting CPCM was dried in air for 48h.

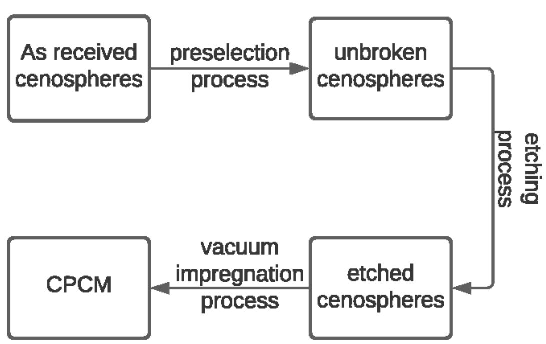

Fig. 1. A schematic flow diagram of the manufacturing process for CPCM

2.2 Bioinspired silica coating on CPCM to produce BCPCM

To apply the bioinspired coating on CPCM, a solution of PAH and Lysozyme referred to as PLS was prepared by dissolving 0.25g of PAH (10mg/ml) and 0.04g of lysozyme in 25 ml of distilled water.

The solution was stirred using a magnetic stirrer at 400 rpm for 2 minutes as depicted in Fig. 2. Subsequently, 5g of CPCM was treated in the PLS solution by mechanical stirring at 1 rpm for 30 min without the application of heat. The mixture was then subjected to vacuum filtration and the filtered treated CPCM was collected. In another beaker, 5 ml $Na_2SiO_3{\cdot}9H_2O$ (1M) solution pre-hydrolyzed with 0.28 g of HCl was prepared and called PHS. The Na2SiO3˙9H2O was pre-hydrolyzed to form silicic acid which the PAH will condense to form silica on the surface of CPCM. The treated CPCM was then added into the PHS solution in the beaker. The pH value of the final solution in the beaker was adjusted with the phosphate buffer solution until pH value reached 7. The resulting mix was mechanically stirred for additional 30 minutes, followed by vacuum filtration to collect the coated microcapsules (BCPCM). The BCPCM samples were then air-dried in a vacuum chamber for further analysis. It is worth noting that this unique coating methodology is environmentally friendly and cost-effective as it does not require the application of heat during the coating process and quick to perform. Additionally, the procedure was carried out at neutral pH, further highlighting its practicality and potential for large-scale implementation. In this bioinspired coating process, the PAH molecules are expected to attach to the surface of the treated CPCM. The presence of PAH facilitates the rapid polycondensation of silica from the pre-hydrolyzed solution, resulting in the formation of silica coating on the surface of the CPCM. This coating effectively seals most of the perforating holes, enhancing the stability of BCPCM and bonding with the concrete matrix.

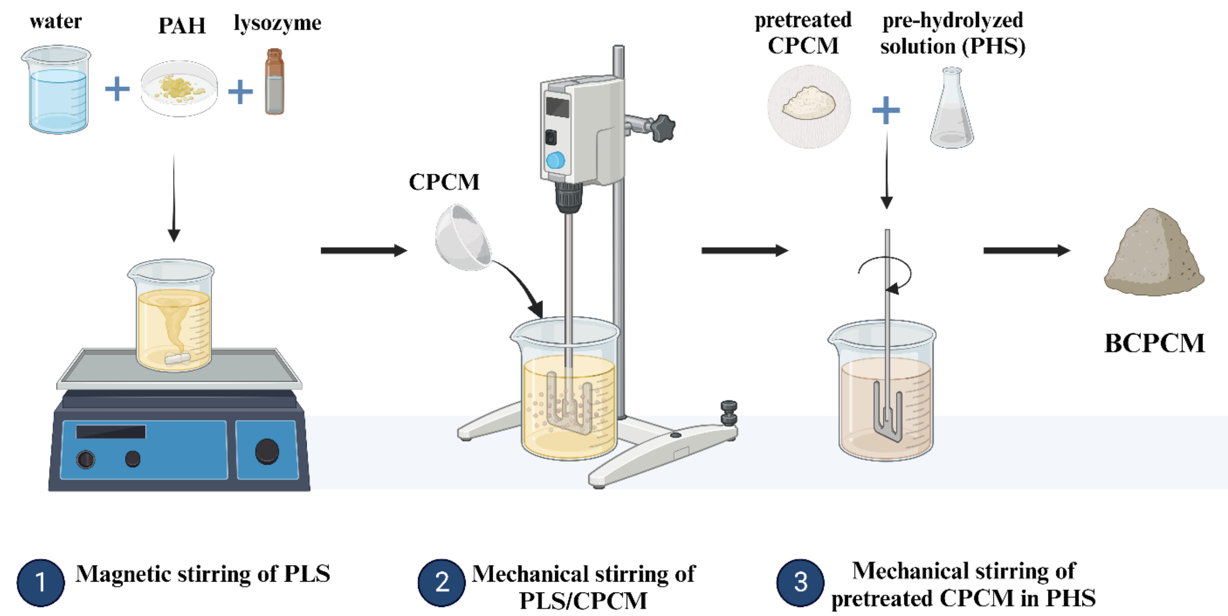

Fig. 2. Process flow diagram of BCPCM production

2.3 Microstructural and chemical characterization

The microstructures of the treated CPCM and BCPCM were studied using Apreo SEM with voltage between 2 and 10 kV and EDS with voltage between 10 and 15 kV. The chemical compatibilities of PCM, PAH, CPCM, treated CPCM, and BCPCM were investigated using FTIR.

2.4 Thermal characterization

The phase change temperatures and latent heats of PCM, CPCM, BCPCM, and cement pastes incorporated with BCPCMs were characterized using TA Instruments Discovery 250 differential DSC. Cement pastes were selected over mortars to allow for micro-sized particles required for the analysis. The scanning rate was set at 5°C/min, and the temperature range investigated was from 0°C to 50°C. The thermal stabilities of the CPCM and BCPCM samples were evaluated using a Q600 TA instrument in thermogravimetric analysis (TGA). To assess the hydration products, TGA tests were conducted on reference mortar samples separately containing CPCM and BCPCM. The heating rate during the TGA test was set to 20°C/min, and the measurements were taken up to 700°C. Using DSC and TGA techniques, the study aimed to determine the phase change properties and thermal stability of the different materials under investigation, shedding light on their potential for thermal energy storage applications in cementitious composites.

2.5 Mortar preparation

The mechanical properties of mortars incorporating CPCM and BCPCM were investigated in this study. The specific gravity of the sand used in the mortar mix was determined to be 2.72 following ASTM C128 [21]. The specific gravities of CPCM and BCPCM were determined to be 1.03 and 1.10, respectively, according to ASTM D 5965 [22]. The mix design for the cement mortars is presented in Table 2. In this design, CPCM or BCPCM were used to fine aggregate, partially substituting the sand content by 0 (control), 10%, 15%, 20%, and 30% in volume. The mortars were mixed as described in [15], then placed in a curing room at 23.0 ± 1.0ºC, and relative humidity of 96%. Compressive strength tests were carried out at 3d, 7d, and 28 d according to ASTM C109 [48]. These tests were performed to evaluate the impact of PCM microcapsules incorporation on the overall strength development of the mortars.

Table 2: Mix proportion of mortar

BCPCM	Cement (g)	Water (g)	Sand (g)	Fine Sand (g)	CPCM (g)	BCPCM (g)
Control	1100	550	1860	1240	0	0
10% vol.	1100	550	1860	930	117	125
15% vol.	1100	550	1860	775	176	188
20% vol.	1100	550	1860	620	235	251
30% vol.	1100	550	1860	310	352	376

2.6 Thermal performance

An in-house experimental setup was fabricated to accurately measure the heat storage and release characteristics of cementitious material as depicted in Fig. 3. The thermally insulated test chamber was constructed with an inner dimension of 1000 mm × 200 mm × 220 mm with a cement board measuring 120 mm × 120 mm × 12 mm placed at 450 mm from the heat source. A 60W infrared lamp was used as the heat source, which provided the necessary thermal energy for the experiments. To ensure a uniform and consistent temperature field, styrofoam boards were positioned on each side of the specimen within the test chamber. Temperature variations at critical locations were recorded using two thermocouples placed at the inner surface of the specimen (point A) and at the center of the test chamber (point B) to mimic indoor conditions. These thermocouples captured and monitored any changes in temperature throughout the course of the experiment. Additionally, a data logger was employed to record the detected temperature variations during each test. The experimental procedure involved activating the heat source for a duration of 85 minutes, after which it was promptly turned off to allowed to cool naturally for 3 h and 30 min. This cooling period enabled the assessment of heat storage and release properties within the specified timeframe, yielding valuable insights into the thermal behavior of cementitious material under investigation.

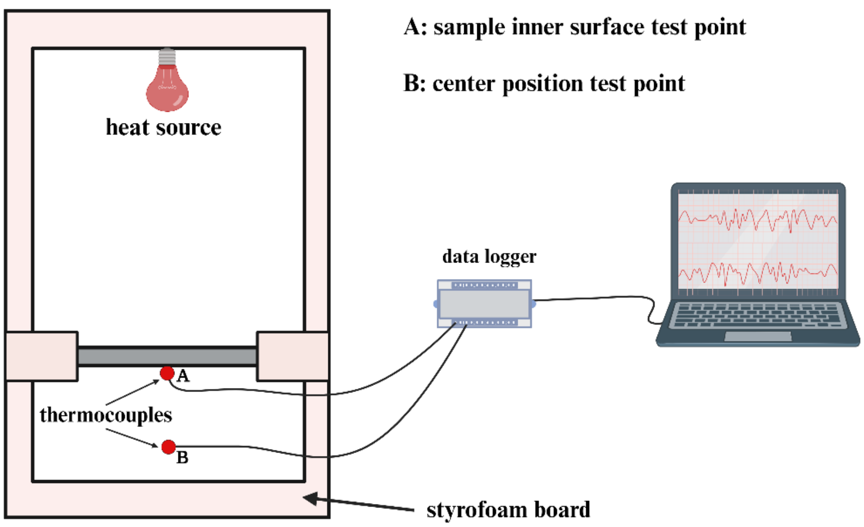

Fig. 3. A schematic representation of the thermal energy storage/release experiment

3. Results and discussions

3.1 Morphology and microstructure of etched cenospheres, CPCM Pretreated CPCM and BCPCM

Fig. 4 presents the SEM images of etched cenosphere, intentionally broken CPCM, treated CPCM, and BCPCM. In Fig. 4(a), the etching process is evident as tiny perforations are observed on the surface of the cenosphere. The etching solution containing HF effectively dissolves the glassy film covering the cenosphere surface without causing harm to the cenospheres. The etched cenosphere exhibits a spongy and textured surface morphology with perforations predominantly ranging from 961 nm to 1.17 μm. These perforations play a vital role in enabling the melted biobased PCM to penetrate into the hollow core of the cenosphere. To evaluate the effectiveness of the vacuum encapsulation process, some CPCMs were intentionally broken (Fig. 4(b)). As depicted, the biobased PCM was successfully loaded into the cenospheres through the visible perforations on the etched surface. This indicates that the etching process not only creates surface punctures but also forms perforations that extend into the hollow section of the cenosphere. Additionally, Fig. 4(b) demonstrates that even after applying pressure to intentionally break the cenospheres, the shell wall remains intact, exposing only a fraction of its inside. The morphology of the CPCM treated in the PLS solution is displayed in Fig. 4(c). Notably, glue-like patches are visible on the surface of the treated CPCMs, indicating the presence of PAH from the PLS solutions on the surface of CPCM as discussed in [23]. This finding highlights the successful attachment of PAH to the surface of CPCM. Fig. 4(d) shows the morphology of BCPCM which differs from what is observed in Fig. 4(c). This disparity arises from the deposition of silica on the surface of the treated CPCM through electrostatic interaction between PAH and silica. The interaction starts with the adsorption of silica nuclei and nanoparticles from the pre-hydrolyzed solution onto the treated CPCM, facilitated by the attractive forces between charged amines on the surface of the treated CPCM and anionic silica species. The coating thickness displayed in Fig. 4(d) varies due to the non-uniform nature of the cenosphere surface and the continuous growth of silica film. However, despite these variations, the coating effectively seals the majority of the perforations that are formed on the etched cenosphere surface. Overall, the SEM analysis provides valuable insights into the morphological characteristics of the etched cenosphere, CPCM, and BCPCM, highlighting the successful encapsulation of the biobased PCM within the cenospheres and the deposition of silica coating on the treated CPCM using the bio-inspired process.

To confirm the presence of PAH on the treated CPCM and the silica coating on BCPCM, EDS analysis was conducted on these samples. Fig. 5(a) presents the EDS spectrum, demonstrating that the cenosphere primarily consists of aluminosilicate with a slightly higher alumina content. This finding aligns with the EDS spectrum of the etched cenosphere and CPCM reported in our previous study [15]. The presence of a small chlorine (Cl) spectrum is observed, originating from the Cl in the PAH (poly allylamine hydrochloride), thereby confirming the presence of PAH patches observed in the SEM image in Fig. 4(c). However, the nitrogen spectrum which would typically arise from the amine group was not detected. This is attributed to the weak response of nitrogen in EDS analysis, making its detection unreliable for many materials [24].

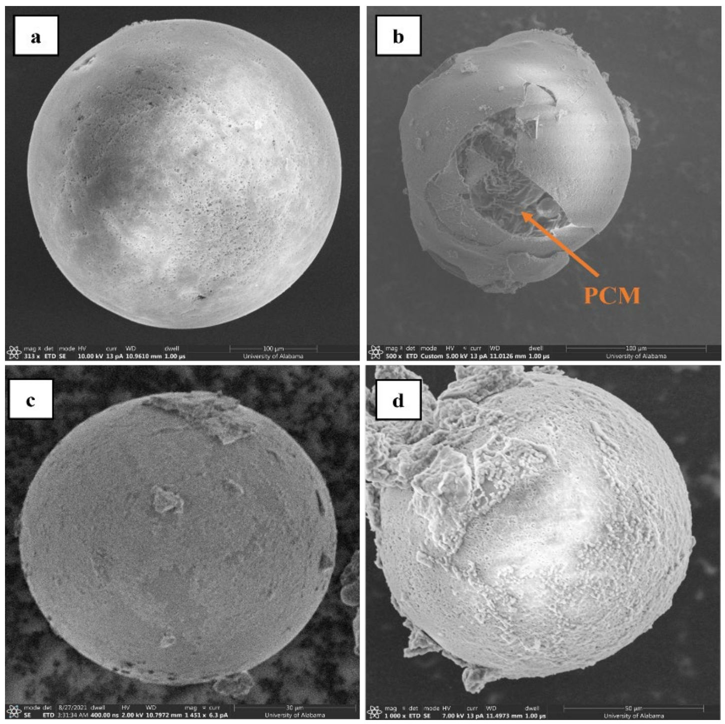

Fig. 4. SEM images of (a) etched cenosphere (b) CPCM (c) pretreated CPCM (d) BCPCM

Fig. 5(b) shows the EDS spectrum for BCPCM. Compared with the spectrum of treated CPCM shown in Fig. 5(a), Fig.5(b) clearly indicates a higher atomic percentage of silicon (Si) in BCPCM, which can be clearly attributed to the silica coating. Furthermore, the presence of small sodium (Na) spectrum can be attributed to some residual pre-hydrolyzed sodium silicate solution that did remain on the surface of the BCPCM after filtration. Similarly, the presence of a small chlorine spectrum can be attributed to the film layer of PAH from the treated CPCM. Nonetheless, the dominant elements observed in the treated CPCM, namely oxygen (O), aluminum (Al), and silicon (Si) still prevail in the BCPCM spectrum. The EDS analysis provides further evidence of the presence of PAH on the treated CPCM and the deposition of silica coating on BCPCM. The observed atomic percentages of the respective elements support these findings, confirming the successful modification of the microcapsule surface and the addition of silica coating.

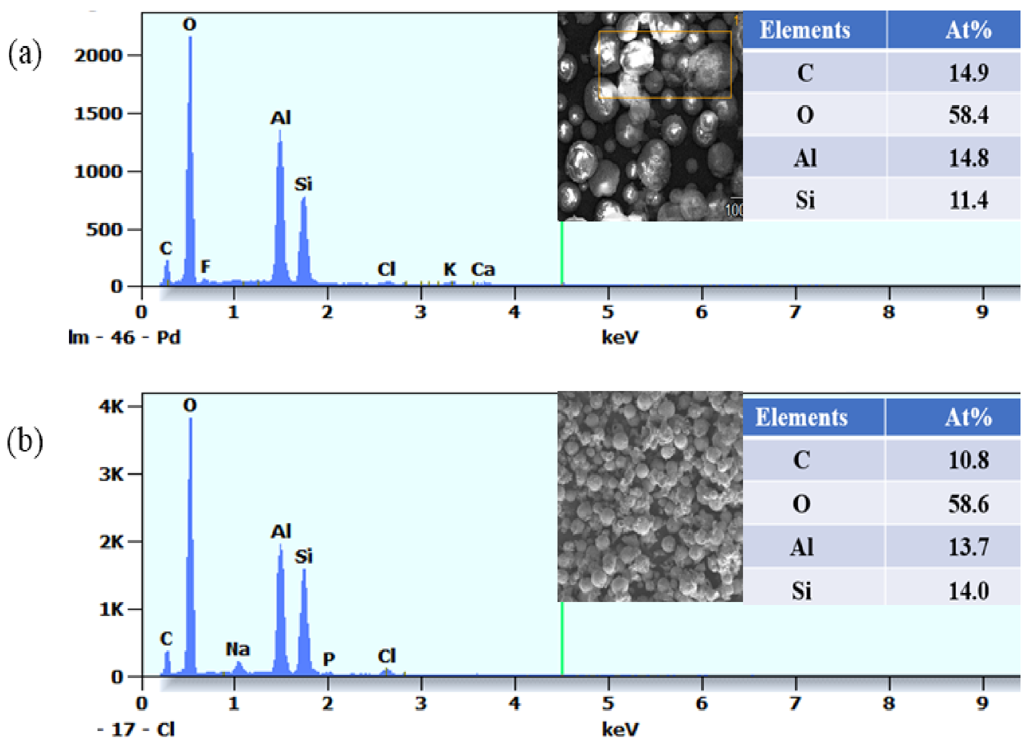

Fig. 5. EDS spectra of (a) pretreated CPCM, (b) BCPCM

3.2. Chemical characterization

The FTIR spectra of the cenosphere, etched cenosphere, PAH, PCM, CPCM, treated CPCM, and BCPCM are presented in Fig. 6. The spectra of the raw cenosphere (Fig. 6(a)) and etched cenosphere (Fig. 6(b)) are similar, suggesting that the chemical etching process does not cause significant damage or alteration to the chemical composition of the original cenospheres. This is not surprising since etching mainly removed the amorphous silica from the cenosphere. The distinctive peaks observed at 1040 cm^{-1} and 738 cm^{-1} in the spectra of these two cenospheres are attributed to the stretching vibrations of Si-O-Si and Si-O bonds [25]. The PAH spectrum (Fig. 6(c)) displays absorption bands related to amide groups, specifically at 1622 cm-1 and 1516 cm-1, which correspond to -NH bending vibration and -CN and -CO stretching, respectively [26]. The bio-based PCM spectrum (Fig. 6(d)) exhibits characteristic peaks associated with -CH groups at 2953 cm^{-1}, 2915 cm^{-1}, and 2846 cm^{-1}. The peak observed at approximately 1739 cm^{-1} is attributed to the presence of the carbonyl group C=O from the carboxylic functional group, while the peaks at 1463 cm^{-1}, 1436 cm^{-1}, 1411 cm^{-1}, and 1000 cm^{-1} are associated with -OH bending [27]. In the spectra of CPCM (Fig. 6(e)), PAH treated CPCM (Fig. 6(f)), and BCPCM (Fig. 6(g)), peaks corresponding to the PCM, cenosphere, and etched cenosphere are evident. The Si-O-Si peaks in the CPCM and BCPCM spectra are observed at reduced intensities, with a more pronounced reduction in the CPCM, which is consistent with the findings of the EDS analysis. This reduction can be attributed to the nonpolar nature and zero net dipole moment of SiO_2 [15]. It is noteworthy that the amide band absorption peaks observed in pure PAH are drastically reduced and almost unnoticeable in the treated CPCM. This is likely due to the biobased PCM film covering most of the surface, as only patches of PAH are present on the pretreated CPCM. The BCPCM spectrum exhibits higher and broader characteristic peaks of Si-O-Si at 1057 cm^{-1} and 1020 cm^{-1} compared to the CPCM. These differences can be attributed to the silica deposition on the BCPCM resulting from the bioinspired coating process. Notably, Fig. 6(g) shows that there is no significant shift in the characteristic peaks of the BCPCM, indicating that it retains all the distinctive bands of each phase. This provides clear evidence that the interaction between the phases is solely a result of physical mixing, and no further chemical reactions occur. Summarily, the results show that silica has been successfully deposited on the surface of the pretreated CPCM, as indicated by the distinctive spectral features observed in the FTIR analysis.

3.3. DSC analysis of PCM, CPCM and BCPCM

One of the primary contributions of this study is the enhancement of the latent heat of coated cenosphere microcapsules compared to our previous work [15]. The DSC curves of PCM, CPCM, and BCPCM are illustrated in Fig. 7. The biobased PCM exhibits latent heat of fusion and crystallization of 213.86 J/g and 207.40 J/g, respectively. The endothermic and exothermic temperature peaks of the biobased PCM were observed at 30.69°C and 23.67°C, respectively. The DSC curve reveals that the CPCM has approximately 56% of its weight occupied by the biobased PCM, as calculated from the CPCM's latent heat of fusion of 119.27 J/g. This corresponds to an impressive loading capacity of the etched cenosphere reaching as high as 127.27% with the biobased PCM. The BCPCM demonstrated latent heat of fusion and crystallization of 86.40 J/g and 85.11 J/g, respectively. This represents an increase in about 31% compared to the coated CPCM reported in our previous study [18]. To confirm the thermal recyclability of the CPCM and BCPCM, 100 thermal cycles were carried out using DSC and the result is as shown in Table 3. It can be seen from the table that even after 100 thermal cycles, the change in latent heat during melting and crystallization for CPCM and BCPCM is almost negligible. However, the deviation of the melting and crystallization temperature is slightly more in CPCM after these thermal cycles attributed to leakage of PCM from the cenosphere. This phenomenon was not observed in BCPCM further confirming its thermal reliability and the effectiveness of the coating to seal most of the perforations on the etched cenospheres.

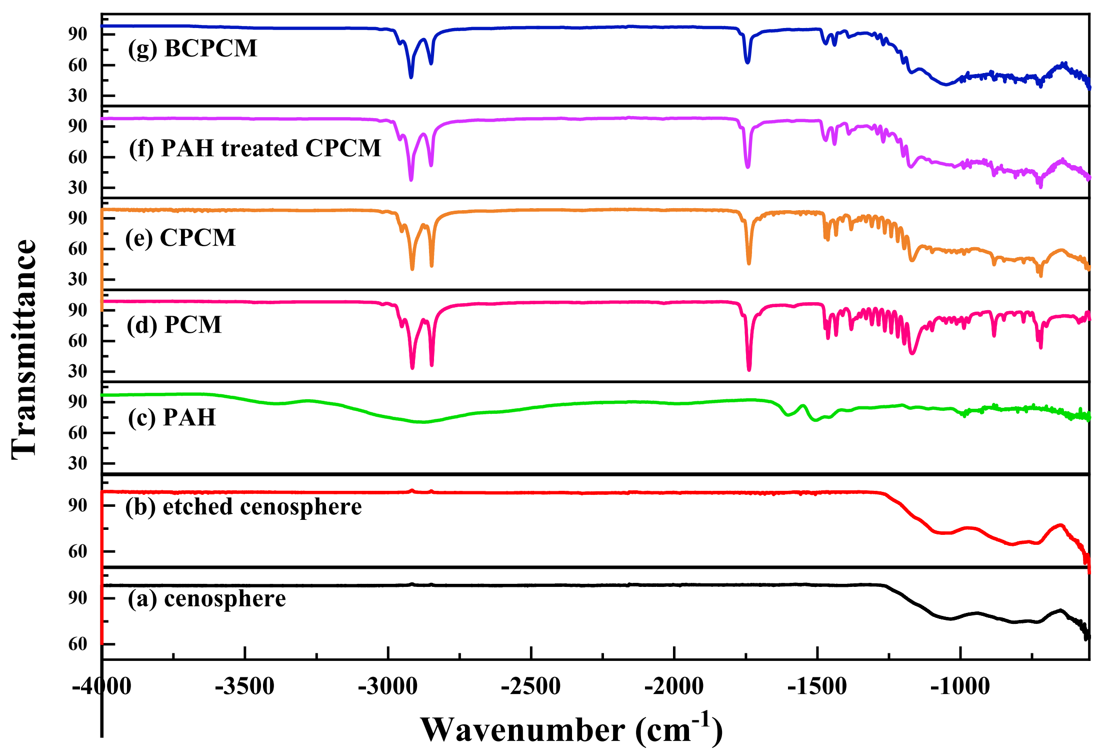

Fig. 6. FTIR spectra of (a) cenosphere, (b) etched cenosphere, (c) PAH (d) PCM, (e) CPCM, (f) pretreated CPCM, (g) BCPCM

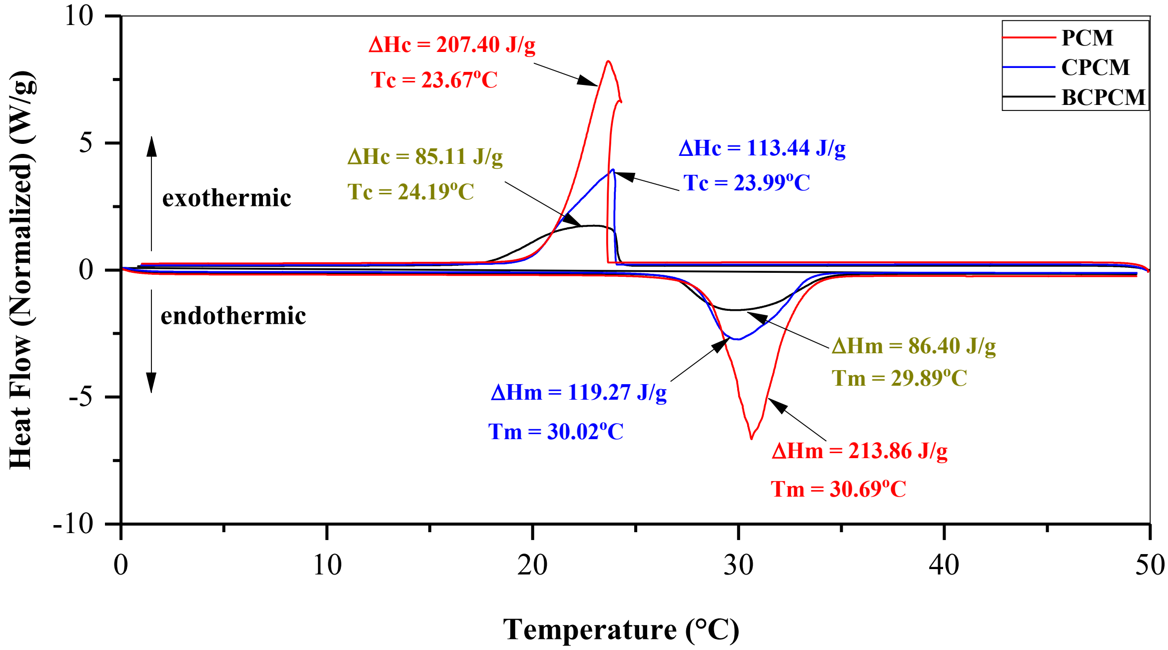

Fig. 7. DSC for PCM, CPCM and BCPCM

Table 3 : Thermal performance of CPCM and BCPCM after 100 thermal cycling

	Melting process				Crystallization process			
	1st thermal cycle		100th thermal cycle		1st thermal cycle		100th thermal cycle	
	Tm (oC)	ΔHm (J/g)	Tm (oC)	ΔHm (J/g)	Tc (oC)	ΔHc (J/g)	Tc (oC)	ΔHc (J/g)
CPCM	30.02	119.27	28.55	118.54	23.99	113.44	25.75	113.69
BCPCM	29.89	86.40	30.01	85.58	24.19	85.11	24.20	86.66

To evaluate the performance of BCPCM, its latent heat is compared with similar studies in literature that have encapsulated biobased PCM in silica-coated cenospheres, as depicted in Fig. 8 previous study [15], [28], [29] . It can be observed that the thermal energy storage capacity of BCPCM is superior, which can be attributed to two possible reasons: (i) this study used water as a solvent instead of organic solvents used in prior studies, which may have led to the dissolution of some PCMs [29] , and (ii) the thin coating developed in this study compared to thick coatings reported previously, which have been identified as a primary factor leading to reduced latent heat in coated cenospheres [15], [28], [29].

The latent heat of cement paste integrated with BCPCMs is also presented in Table 4. It is evident from the table that the transition temperatures of BCPCM pastes at different incorporation levels are relatively close with minimal deviation from the DSC results of BCPCM and pure biobased PCM shown in Fig. 6. This indicates that the phase change properties of BCPCM remain unaffected when integrated into cementitious composite. As the ratio of BCPCM increases, the latent heat of paste also increases. However, for BCPCMs below 20% incorporation, there is a noticeable difference between theoretical and tested latent heat values.]

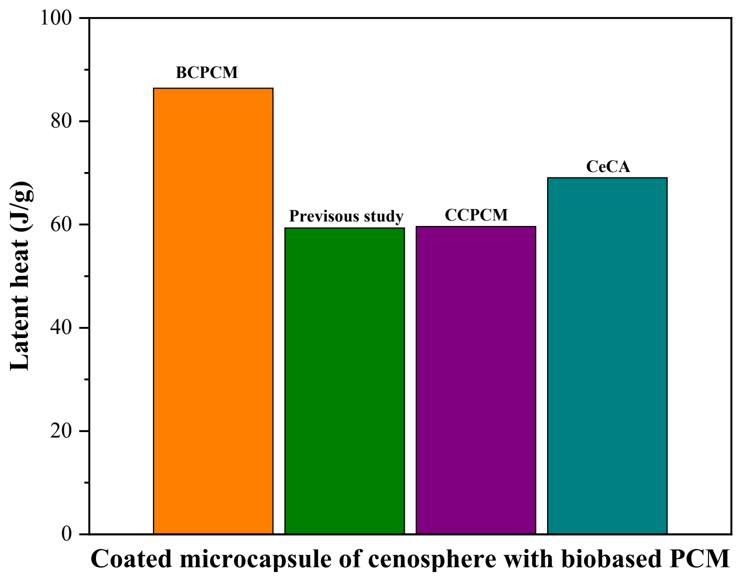

Fig. 8. A comparison of the latent heat of BCPCM with similar studies in the literature [15], [28], [29]

This discrepancy could be attributed to the lower volume of microcapsules in cementitious matrix at the given incorporation levels or non-uniformity in the tested samples. Nevertheless, at all incorporation levels, BCPCM contributes to the enhanced thermal performance of cementitious composite.

Table 4: Latent heat of cementitious composite with BCPCMs

	Melting temp. (ºC)	Freezing temp. (ºC)	ΔH_m (Theoretical, J/g)	ΔH_m (Tested, J/g)	% Diff.

10% BCPCM	28.65	20.42	5.50	4.0	27.0%
15% BCPCM	28.58	19.98	8.27	5.1	38.0%
20% BCPCM	29.25	20.32	11.0	10.0	9.1%
30% BCPCM	30.14	20.42	16.5	16.2	1.8%

3.4 Thermal stability of BCPCM

The thermal stability of BCPCM was assessed by TGA. The thermal decomposition of CPCM, as depicted in Fig. 9(a), initiated at approximately 135°C, accompanied by a weight loss attributed to the degradation of the PCM. This weight reduction continued gradually until around 270°C. Subsequently, the weight remained constant until the end of the test, indicating the thermally stable nature of the cenosphere shell which does not undergo further decomposition.

The DTG curve for CPCM, shown in Fig. 9(b), demonstrates the complete decomposition of the PCM by 270°C and no peak afterwards, confirming the thermal stability of the cenosphere. In the TGA and DTG curves, a sudden percentage weight loss of about 3.5% is observed till about 170°C in BCPCM, which can be attributed to the moisture content attached to the silica [30]. The decomposition of the PCM in BCPCM is delayed by approximately 50°C compared to CPCM, as evident in Fig. 9(a), owing to the presence of the coating on the surface of BCPCM. This delay is clearly depicted as a peak shift to the right in the DTG curve (Fig. 9(b)). This delay in thermal decomposition by coating can help with fire resistance by shielding and preventing early leakage of the melted PCM [31]. The TGA analysis indicates that the PCM accounts for 42% of the total weight, corresponding to approximately 89 J/g. This result aligns with the high latent heat of BCPCM reported in DSC analysis. The minor hump observed in Fig. 9(a) and the peaks in Fig. 9(b) between 300°C and 400°C for BCPCM are attributed to the decomposition of some coating material. The residual wt.% increase of about 11.7% of the BCPCM compared to the CPCM is from the silica. This is much lower than the 19.6 wt.% of silica coating reported in our previous study, indicating that the coating in BCPCM is thinner. This thin coating could contribute to the enhanced latent heat of BCPCM. No further decomposition was observed after 500°C as seen in both the TGA and DTG curves.

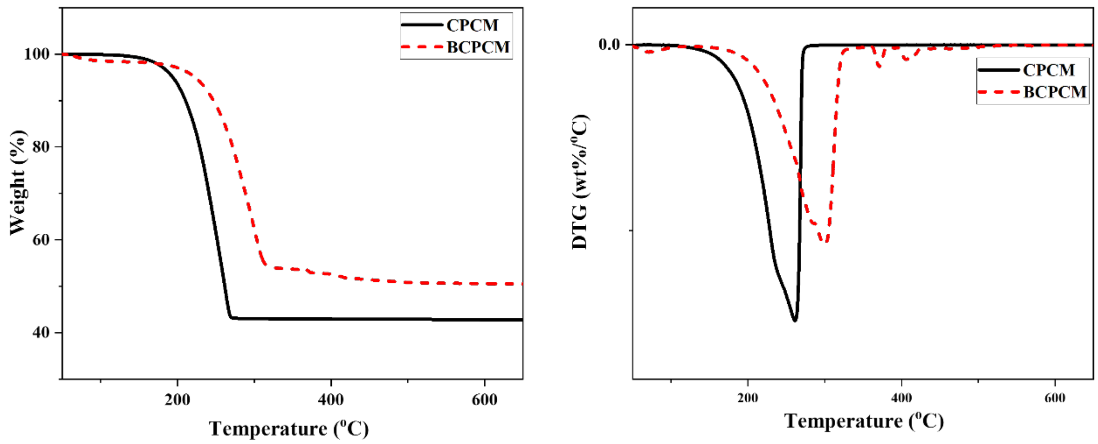

(a) (b)

Fig. 9. (a) TGA thermogragh of CPCM and BCPCM, (b) DTG curve for CPCM and BCPCM

3.5 Compressive strength

The compressive strength of the mortar was evaluated to assess its mechanical performance at various incorporation levels of CPCM and BCPCM. The compressive strengths at 3d, 7d, and 28d were determined. As shown in Fig. 10, the strengths of the mortars increased with age for the control and all microcapsule incorporated composites. As expected, the compressive strength of the mortar containing CPCM decreased as the volume percentage of CPCM increased. This reduction ranges between 24-37.9% compared to the reference sample. The reference mortar exhibited a compressive strength of 59.84 MPa, while the lowest compressive strength observed for the mortar with a 30% volume of sand replacement by CPCM was 37.15 MPa. This decrease in strength can be attributed to the lower crushing strength of cenospheres compared to the sand it replaced [32], and there is also a possibility of PCM leakage into the cementitious composites, which may have a detrimental effect on the mortar. Despite this reduction in strength , the 28d strength of the mortar with CPCM is still sufficiently high for structural, plastering, or masonry applications [33]. The compressive strength of the mortar with BCPCM is depicted in Fig. 10(b). Similar to the observations with CPCM, the compressive strength of the mortar decreased as the amount of BCPCM increased. However, the reduction in compressive strength for BCPCM mortar ranged from 15-31%, which is significantly lower compared to the reduction observed with CPCM. The use of the bioinspired coating on BCPCM resulted in the recovery of some of compressive strength loss observed in the mortar with CPCM. As shown in Fig. 11, the coating enhanced the strengths of the mortars with 10%, 15%, 20%, and 30% volume of sand replaced by CPCM by 12.45%, 14.31%, 28.3%, and 11.0%, respectively. The reasons responsible for this increased strength can be summarized as follows: Several factors contributed to this increased strength: (i) The presence of the silica coating on the surface of BCPCM facilitated the formation of a greater amount of C-S-H gel, which is known to enhance the strength and durability of cementitious materials. (ii) The bioinspired coating effectively minimized or prevented leakage of the biobased PCM into the cementitious composite matrix. This prevented any potential adverse effects that PCM leakage may have on the mortar and maintained the structural integrity of the composite [39]. Similar increases in compressive strength due to silica coating have been reported in the literature [15], [28].

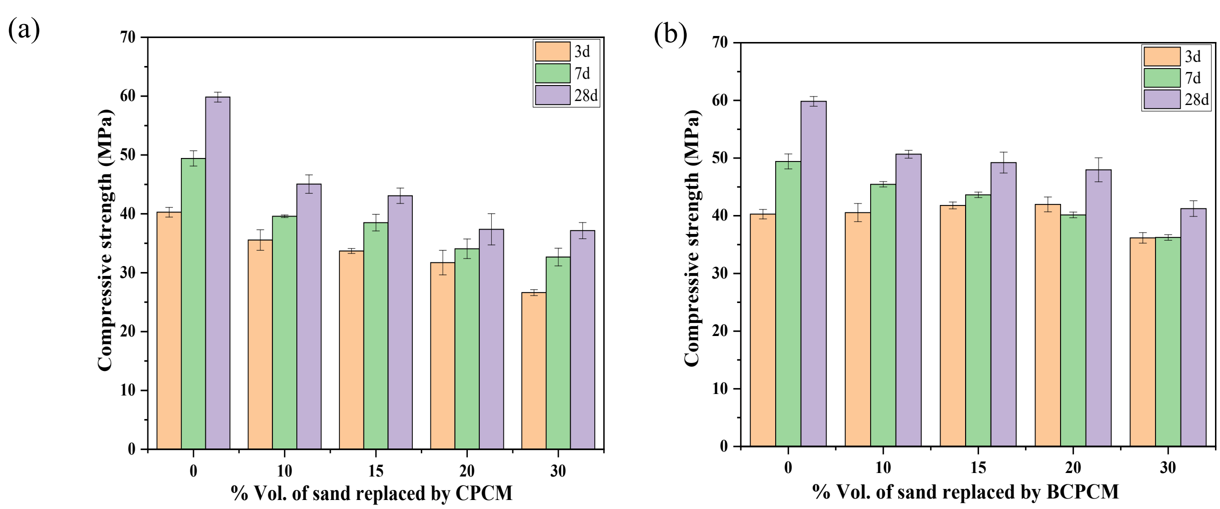

Fig. 10. Compressive strength of (a) cement mortars with and without CPCM; (b) cement mortars with and without BCPCM

The mechanical performance of mortars with BCPCM is compared with those reported in other studies available in the literature as shown in Table 5 [15], [34]–[41]. It can be observed that the mechanical performance of mortars incorporating BCPCM is superior at all levels of incorporation compared to the mortars reported in the literature, with the exception of our previous study [18]. This is not surprising since the cenosphere shell is much stronger than any other shells used in the literature. The superior mechanical performance of cenosphere shell makes it possible to incorporate high volume of PCM microcapsule in the mortar. When 30% of sand was replaced by the BCPCM, the mortar still retains over 60% of the compressive strength at 28d. As a comparsion, mortars developed by Tian et al [34] lost almost 90% of its strength. Table 4 also suggests that the strength of the mortar with BCPCM is slightly lower than the one presented in our previous study [18]. This can be attributed to the fact that the silica layer on the cenosphere from our previous study is much thicker than that of the BCPCM, thereby contributing more to the formation of C-S-H for improved compressive strength. This result further confirms the thinness of the bioinspired silica coating, the increased latent heat observed and the superior mechanical performance of cenospheres as microcapsules for PCMs.

Table 5: Comparison of 28d Compressive strengths of MPCMs in mortars reported in the literature

Studies	% MPCM in cementitious material	~ % 28d compressive strength reduction*	Ref.
Tian et. al	10, 20, 30	27, 49, 88	[34]
Haider et. al	10, 15	43, 50	[35]
Aguayo et. al	10, 15, 20	20, 37, 39	[36]
Gbekou et al	10, 15, 20	76, 83, 88	[37]
Illampas et. al	10, 15	65, 78	[38]
Zhang et. al	10, 20	17, 36	[39]
Gencel et. al	10, 15	17, 40	[40]
Cui et. al	10, 20	24, 44	[41]
Previous study	10, 15, 20, 30	2 (increase), 4, 14, 24	[15]
This study	10, 15, 20, 30	15, 18, 20, 31	

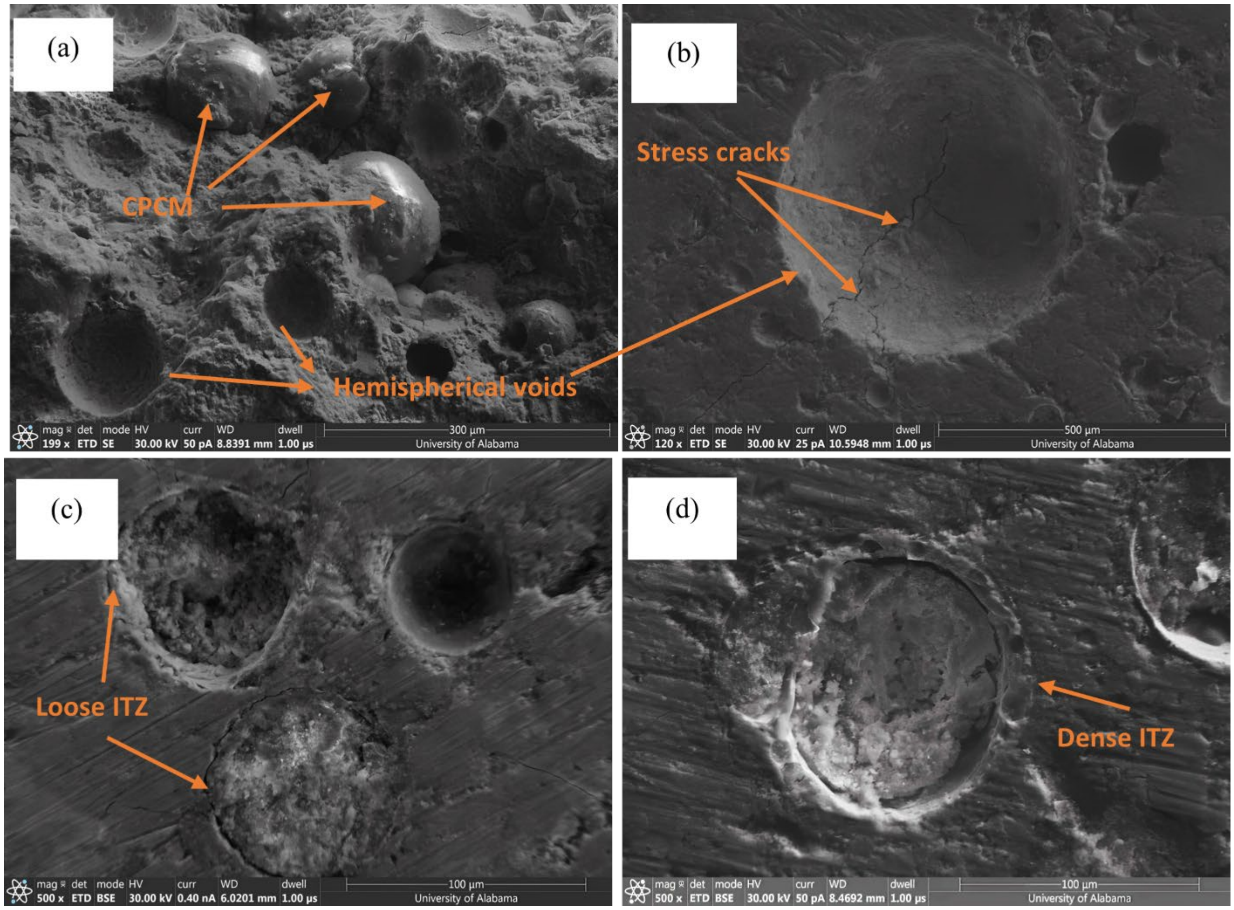

Fig. 11. (a), (b) SEM image of mortar integrated with cenosphere microcapsules; (c) BSE image of the mortar with CPCM; (d) BSE image of the mortar with BCPCM

After conducting the compression test, the mortar particles containing CPCM and BCPCM were collected and analyzed using scanning electron microscopy (SEM), as illustrated in Fig. 11. The SEM image in Fig. 11(a) reveals that cenospheres were evenly dispersed throughout the mortar. These PCM microcapsules occupied some of the hemispherical spaces before the compression test. However, during the test, these PCM microcapsules were forcibly ripped out, resulting in damage and the formation of observed hemispherical voids and the stress cracks seen in Fig. 11(b). Remarkably, these cenosphere microcapsules maintained their structural integrity without shattering or deforming during the mixing process, highlighting their excellent mechanical performance. This supports the excellent mechanical performance of cenosphere microcapsules even further. The backscattered electron (BSE) image of samples with CPCM, Fig. 11(c), show cracks around the loose interfacial transition zone (ITZ) between CPCM and the cementitious matrix, which can be attributed to the leakage of the PCM from the cenosphere. However, the ITZ observed in Fig. 11(d) appears dense and free of cracks. This observation further confirms the effectiveness of the bioinspired silica coating in preventing PCM leakage. It also provides evidence supporting the strength improvement achieved through the application of the coating, as demonstrated in Fig. 10.

3.6 Thermal energy storage and release

The temperature evolution curves at the inner surface of the paste sample and the center of the cubic space behind the paste sample are presented in Figs.12(a) and 12(b), respectively, for the control paste and pastes containing different quantities of BCPCMs. The temperature peak of the control sample, as observed in Fig. 12(a), is significantly higher compared to the paste samples incorporating BCPCM. Moreover, as the quantity of BCPCM increases, there is a gradual reduction in the temperature peak. During the heating period, as depicted in Fig. 12(a), the incorporation of increasing amounts of BCPCM leads to a slower temperature rise and a slight shift in the peaks to the right when the PCM begins to melt at temperatures ranging between 28°C and 31°C. This observation indicates that both the temperature peak and the rate of temperature increase decrease with higher BCPCM content, thereby highlighting a substantial enhancement in thermal energy storage capacity. The cooling phase of the curve exhibits similar trend to the heating period. The temperature of the control sample exhibits a rapid decrease, whereas the samples incorporating BCPCM demonstrate slower cooling rates and maintain temperatures above that of the control sample for approximately 160 minutes during the cooling period, which is close to the phase transition temperature of the PCM. Similar results were observed in Fig. 12(b), where the indoor temperatures were cooler compared to the surface temperatures as the amounts of BCPCM increased. The temperature peaks and differences at different testing points on the samples are presented in Table 6. For point A, which represents the sample surface, the temperatures decreased by 1.63°C, 4.87°C, 6.34°C, and 7.92°C with the incorporation of 10%, 15%, 20%, and 30% BCPCM, respectively. Similarly, at point B, which represents the center of the sample, the temperatures decreased as the amount of BCPCM increased. These findings clearly demonstrate the significant TES potential of PCM when incorporated into construction materials, as well as the ability of BCPCM to enhance and regulate indoor temperatures effectively.

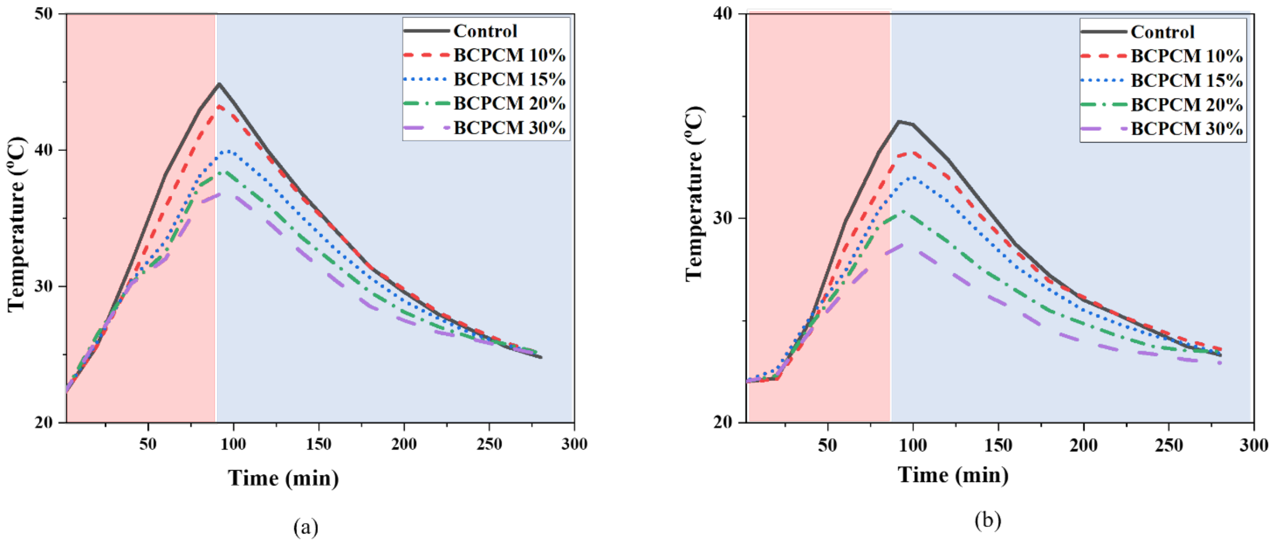

Fig. 12. (a) Temperature evolutions of the paste containing BCPCM (a) back of sample, (b) center position representing indoor

Table 6. Temperature peaks and reductions at different testing positions

BCPCM %	Peak temperature at A (°C)	The temperature reduction at A (°C)	Peak temperature at B (°C)	The temperature reduction at B(°C)
0	44.86	-	34.73	-
10	43.23	-1.63	33.06	-1.67
15	39.99	-4.87	31.83	-2.90
20	38.52	-6.34	30.34	-4.39
30	36.94	-7.92	28.76	-5.97

4. Conclusions

In conclusion, this study introduces a novel bioinspired method for applying a silica coating on the surface of CPCM microcapsules, offering several key advantages over existing methods. The new coating technique is performed under mild pH and ambient temperature conditions, making it environmentally friendly and cost-effective. The utilization of low-cost sodium silicate as a precursor further enhances its economic feasibility. The developed silica-coated, cenosphere-based PCM microcapsules (BCPCM) exhibit promising properties and present significant contributions to sustainable building materials.

The successful deposition of the bioinspired silica coating on the CPCM microcapsules effectively seals perforations on the etched cenospheres, resulting in improved thermal performance. The analysis reveals a remarkable 31% increase in the latent heat of BCPCM compared to previous studies. The enhanced thermal stability of BCPCM, demonstrated by a delayed thermal decomposition of PCM by approximately 50°C, offers improved fire resistance and mitigates early leakage of PCM. Although the incorporation of both CPCM and BCPCM slightly reduces the compressive strength of the mortar, BCPCM exhibits a significantly lower reduction compared to CPCM and other existing technologies. The bioinspired silica coating contributes to the recovery of strength loss, restoring a notable percentage of strength reduction caused by the incorporation of different amounts of CPCM into the mortar. Additionally, the coating facilitates the formation of a dense interfacial transition zone (ITZ) layer between BCPCM and the cementitious matrix, enhancing the overall performance of the composite material. Furthermore, BCPCM demonstrates improved thermal energy storage and temperature control capabilities, making it suitable for managing thermal demands in buildings. The potential application of BCPCM can be in concrete, mortar, plasters and building products such as paints, roof tiles, floor tiles, acoustic walls, and dry walls, for enhanced thermal performance.

Overall, BCPCM provides a superior solution to integrate thermal energy storage into cementitious material. Very high-volume substitution (30%) of aggregates with BCPCM can be reached by this PCM microcapsule without loss most of its strength, which cannot be achieved by any existing MPCM with polymer shell.

Declaration of competing interest

The authors declare that there is no known competing financial or personal interest that could have appeared to influence the work reported in this paper.

Acknowledgments

This indispensable financial support by the U.S. Department of Energy (DOE) Building Technology Office (DE-EE-0008677) and National Science Foundation (CMMI-1563551, IIP-2118493) is greatly appreciated. This work was co-authored by the National Renewable Energy Laboratory, operated by Alliance for Sustainable Energy, LLC, for the U.S. Department of Energy (DOE) under Contract No. DE-AC36-08GO28308. The views expressed in the article do not necessarily represent the views of the DOE or the U.S. Government. The U.S. Government retains and the publisher, by accepting the article for publication, acknowledges that the U.S. Government retains a nonexclusive, paid-up, irrevocable, worldwide license to publish or reproduce the published form of this work, or allow others to do so, for U.S. Government purposes.

Declaration of generative AI and AI-assisted technologies in the writing process

During the preparation of this work the author(s) used ChatGPT in order to improve language. After using this tool/service, the author(s) reviewed and edited the content as needed and take(s) full responsibility for the content of the publication.

References

[1] M. M. Umair, Y. Zhang, K. Iqbal, S. Zhang, and B. Tang, "Novel strategies and supporting materials applied to shape-stabilize organic phase change materials for thermal energy storage–A review," *Appl Energy*, vol. 235, pp. 846–873, 2019.

[2] A. M. Borreguero, J. L. Valverde, J. F. Rodríguez, A. H. Barber, J. J. Cubillo, and M. Carmona, "Synthesis and characterization of microcapsules containing Rubitherm® RT27 obtained by spray drying," *Chemical Engineering Journal*, vol. 166, no. 1, pp. 384–390, 2011.

[3] W. Li, G. Song, G. Tang, X. Chu, S. Ma, and C. Liu, "Morphology, structure and thermal stability of microencapsulated phase change material with copolymer shell," *Energy*, vol. 36, no. 2, pp. 785–791, 2011.

[4] G. Enteshari and E. Najafi Kani, “Fabrication and Performance of Microencapsulated Phase-Change Material/Gypsum Plaster Tile for Thermal Energy–Storage Building Material,” *Journal of Materials in Civil Engineering*, vol. 34, no. 5, 2022.

[5] C. Liu, H. Cao, S. Jin, Y. Bao, Q. Cheng, and Z. Rao, “Synthesis and characterization of microencapsulated phase change material with phenol-formaldehyde resin shell for thermal energy storage,” *Solar Energy Materials and Solar Cells*, vol. 243, no. 111789, 2022.

[6] L. Zhao, H. Wang, J. Luo, Y. Liu, G. Song, and G. Tang, “Fabrication and properties of microencapsulated n-octadecane with TiO2 shell as thermal energy storage materials,” *Solar Energy*, vol. 127, pp. 28–35, 2016.

[7] J. Giro-Paloma, M. Martínez, L. F. Cabeza, and A. I. Fernández, “Types, methods, techniques, and applications for microencapsulated phase change materials (MPCM): A review,” *Renewable and Sustainable Energy Reviews*, vol. 53, 2016.

[8] M. Hunger, A. G. Entrop, I. Mandilaras, H. J. H. Brouwers, and M. Founti, “The behavior of self-compacting concrete containing micro-encapsulated Phase Change Materials,” *Cem Concr Compos*, vol. 31, no. 10, pp. 731–743, Nov. 2009.

[9] F. Li, X. Wang, and D. Wu, “Fabrication of multifunctional microcapsules containing n-eicosane core and zinc oxide shell for low-temperature energy storage, photocatalysis, and antibiosis,” *Energy Convers Manag*, vol. 106, pp. 873–885, 2015.

[10] L. Chai, X. Wang, and D. Wu, “Development of bifunctional microencapsulated phase change materials with crystalline titanium dioxide shell for latent-heat storage and photocatalytic effectiveness,” *Appl Energy*, vol. 138, pp. 661–674, 2015.

[11] Z. Zhang, Y. Lian, X. Xu, X. Xu, G. Fang, and M. Gu, “Synthesis and characterization of microencapsulated sodium sulfate decahydrate as phase change energy storage materials,” *Appl Energy*, vol. 255, no. 113830, 2019, doi: doi.org/10.1016/j.apenergy.2019.113830.

[12] Z. Jiang *et al.*, “Microencapsulated paraffin phase-change material with calcium carbonate shell for thermal energy storage and solar-thermal conversion,” *Langmuir*, vol. 34, no. 47, pp. 14254–14264, 2018.

[13] D. J. ; Corr and S. P. ; Shah, “Design and Application of High-Volume Fly Ash Self-Consolidating Concrete with the Incorporation of Nanoparticles.".” 2012. Accessed: Jul. 01, 2023. [Online]. Available: https://rosap.ntl.bts.gov/view/dot/39247

[14] A. Ismail, J. Wang, B. Abiodun Salami, L. O. Oyedele, and G. K. Otukogbe, “Microencapsulated phase change materials for enhanced thermal energy storage performance in construction materials: A critical review,” *Constr Build Mater*, vol. 401, p. 132877, Oct. 2023, doi: 10.1016/j.conbuildmat.2023.132877.

[15] A. Ismail, J. Zhou, A. Aday, I. Davidoff, A. Odukomaiya, and J. Wang, “Microencapsulation of bio-based phase change materials with silica coated inorganic shell for thermal energy storage,” *Journal of Building Engineering*, vol. 67, 2023, doi: 10.1016/j.jobe.2023.105981.

[16] X. Wang, C. Li, and T. Zhao, “Fabrication and characterization of poly (melamine-formaldehyde)/silicon carbide hybrid microencapsulated phase change materials with enhanced

thermal conductivity and light-heat performance," *Solar Energy Materials and Solar Cells*, vol. 2, 2018.

[17] W. E. G. Müller *et al.*, "Molecular Mechanism of Spicule Formation in the Demosponge Suberites domuncula: Silicatein-Collagen-Myotrophin," 2003. doi: 10.1007/978-3-642-55486-5_8.

[18] M. Sumper and N. Kröger, "Silica formation in diatoms: The function of long-chain polyamines and silaffins," *Journal of Materials Chemistry*, vol. 14, no. 14. 2004. doi: 10.1039/b401028k.

[19] M. Hildebrand, "Diatoms, biomineralization processes, and genomics," *Chem Rev*, vol. 108, no. 11, 2008, doi: 10.1021/cr078253z.

[20] S. V. Patwardhan, "Biomimetic and bioinspired silica: Recent developments and applications," *Chemical Communications*, vol. 47, no. 27. 2011. doi: 10.1039/c0cc05648k.

[21] "Standard Test Method for Relative Density (Specific Gravity) and Absorption of Fine Aggregate 1", doi: 10.1520/C0128-15.

[22] "Standard Test Method for Specific Gravity of Coating powders ASTM D5965-02," *ASTM International*, Dec. 2012, doi: 10.1520/D5965-19.

[23] S. D. Pogula, S. V. Patwardhan, C. C. Perry, J. W. Gillespie, ShridharpYarlagadda, and K. L. Kiick, "Continuous silica coatings on glass fibers via bioinspired approaches," *Langmuir*, vol. 23, no. 12, pp. 6677–6683, Jun. 2007, doi: 10.1021/la063685a.

[24] W. J. Wolfgong, "Chemical analysis techniques for failure analysis," in *Handbook of Materials Failure Analysis with Case Studies from the Aerospace and Automotive Industries*, Elsevier, 2016, pp. 279–307. doi: 10.1016/B978-0-12-800950-5.00014-4.

[25] H. Kaya, D. Ngo, S. Gin, and S. H. Kim, "Spectral changes in Si–O–Si stretching band of porous glass network upon ingress of water," *J Non Cryst Solids*, vol. 527, p. 119722, Jan. 2020, doi: 10.1016/j.jnoncrysol.2019.119722.

[26] M. Elahi, G. Guan, L. Wang, and M. King, "Influence of Layer-by-Layer Polyelectrolyte Deposition and EDC/NHS Activated Heparin Immobilization onto Silk Fibroin Fabric," *Materials*, vol. 7, no. 4, pp. 2956–2977, Apr. 2014, doi: 10.3390/ma7042956.

[27] W. Zhang *et al.*, "Preparation and characterization of capric-palmitic-stearic acid ternary eutectic mixture/expanded vermiculite composites as form-stabilized thermal energy storage materials," *J Mater Sci Technol*, vol. 34, no. 2, pp. 379–386, Feb. 2018, doi: 10.1016/j.jmst.2017.06.003.

[28] A. L. Brooks, Y. Fang, Z. Shen, J. Wang, and H. Zhou, "Enabling high-strength cement-based materials for thermal energy storage via fly-ash cenosphere encapsulated phase change materials," *Cem Concr Compos*, vol. 120, no. 104033.

[29] S. Perumal Arulselvan and S. Vellalapalayam Gurusamy, "Characterization of Fly Ash Cenosphere – Capric acid composite as phase change material for thermal energy storage in buildings," *Energy Sources, Part A: Recovery, Utilization, and Environmental Effects*, vol. 44, no. 1, pp. 2088–2102, Mar. 2022, doi: 10.1080/15567036.2022.2055234.

[30] J. Azadmanjiri, G. P. Simon, K. Suzuki, C. Selomulya, and J. D. Cashion, "Phase reduction of coated maghemite (γ-Fe_2O_3) nanoparticles under microwave-induced plasma heating for rapid heat treatment," *J. Mater. Chem.*, vol. 22, no. 2, pp. 617–625, 2012, doi: 10.1039/C1JM12524A.

[31] M. F. Saleem, W. Khaliq, R. A. Khushnood, M. Rizwan, and H. Sardar, “Shielding Encapsulation to Enhance Fire Endurance of Phase Change Materials in Energy-Efficient Concrete,” *Fire Technol*, Apr. 2023, doi: 10.1007/s10694-023-01404-9.

[32] F. Liu, J. Wang, and X. Qian, “Integrating phase change materials into concrete through microencapsulation using cenospheres,” *Cem Concr Compos*, vol. 80, pp. 317–325.

[33] A. Marani and M. L. Nehdi, “Integrating phase change materials in construction materials: Critical review,” *Constr Build Mater*, vol. 217, pp. 36–49.

[34] Y. Tian, Y. Lai, W. Pei, Z. Qin, and H. Li, “Study on the physical mechanical properties and freeze-thaw resistance of artificial phase change aggregates,” *Constr Build Mater*, vol. 329, Apr. 2022, doi: 10.1016/j.conbuildmat.2022.127225.

[35] M. Z. Haider, X. Jin, and J. W. Hu, “Development of nanomodified-cementitious composite using phase change material for energy saving applications,” *Appl Energy*, vol. 340, Jun. 2023, doi: 10.1016/j.apenergy.2023.121067.

[36] M. Aguayo *et al.*, “‘The influence of microencapsulated phase change material (PCM) characteristics on the microstructure and strength of cementitious composites: Experiments and finite,’” *Cement and Concrete Composites*, vol. 73. pp. 29–41, 2016. doi.org/10.1016/j.cemconcomp.2016.06.018.

[37] F. K. Gbekou, K. Benzarti, A. Boudenne, A. Eddhahak, and M. Duc, “Mechanical and thermophysical properties of cement mortars including bio-based microencapsulated phase change materials,” *Constr Build Mater*, vol. 352, Oct. 2022, doi: 10.1016/j.conbuildmat.2022.129056.

[38] R. Illampas, I. Rigopoulos, and I. Ioannou, “Influence of microencapsulated Phase Change Materials (PCMs) on the properties of polymer modified cementitious repair mortar,” *Journal of Building Engineering*, vol. 40, no. 102328, 2021.

[39] N. Zhang *et al.*, “Preparation and performance of multifunctional pumping wet shotcrete with the inclusion of microencapsulated phase change material,” *Case Studies in Thermal Engineering*, vol. 37, Sep. 2022, doi: 10.1016/j.csite.2022.102277.

[40] O. Gencel *et al.*, “Microencapsulated phase change material incorporated light transmitting gypsum composite for thermal energy saving in buildings,” *J Energy Storage*, vol. 67, p. 107457, Sep. 2023, doi: 10.1016/j.est.2023.107457.

[41] H. Cui, S. Yu, X. Cao, and H. Yang, “Evaluation of Printability and Thermal Properties of 3D Printed Concrete Mixed with Phase Change Materials,” *Energies (Basel)*, vol. 15, no. 6, Mar. 2022, doi: 10.3390/en15061978.